

Article

# Aerodynamic Performance of a NREL S809 Airfoil in an Air-Sand Particle Two-Phase Flow

Dimitra C. Douvi \*, Dionissios P. Margaris \* and Aristeidis E. Davaris

Fluid Mechanics Laboratory (FML), Mechanical Engineering and Aeronautics Department, University of Patras, GR-26500 Patras, Greece; c1.davar@gmail.com

\* Correspondence: dimdouvi@gmail.com (D.C.D.); margaris@mech.upatras.gr (D.P.M.)

Academic Editor: Demos T. Tsahalis

Received: 12 December 2016; Accepted: 6 February 2017; Published: 28 February 2017

**Abstract:** This paper opens up a new perspective on the aerodynamic performance of a wind turbine airfoil. More specifically, the paper deals with a steady, incompressible two-phase flow, consisting of air and two different concentrations of sand particles, over an airfoil from the National Renewable Energy Laboratory, NREL S809. The numerical simulations were performed on turbulence models for aerodynamic operations using commercial computational fluid dynamics (CFD) code. The computational results obtained for the aerodynamic performance of an S809 airfoil at various angles of attack operating at Reynolds numbers of  $Re = 1 \times 10^6$  and  $Re = 2 \times 10^6$  in a dry, dusty environment were compared with existing experimental data on air flow over an S809 airfoil from reliable sources. Notably, a structured mesh consisting of 80,000 cells had already been identified as the most appropriate for numerical simulations. Finally, it was concluded that sand concentration significantly affected the aerodynamic performance of the airfoil; there was an increase in the values of the predicted drag coefficients, as well as a decrease in the values of the predicted lift coefficients caused by increasing concentrations of sand particles. The region around the airfoil was studied by using contours of static pressure and discrete phase model (DPM) concentration.

**Keywords:** aerodynamic performance; S809; airfoil; two-phase flow; sand particles; CFD code

---

## 1. Introduction

In the last few years, renewable sources of energy have been used extensively in many applications, such as power generation. Renewable sources of energy are significantly superior to fossil energy, due to the fact that they are free and abundant and have a low impact on the environment. Specifically, wind energy is becoming more important every year and, therefore, wind power generators have attracted a great deal of attention from research teams in pursuing optimal aerodynamic performance.

The aerodynamic performance of wind turbine blades can be affected by many conditions, such as sand concentration in dry, dusty environments. Although much research has been conducted on the detrimental effects of certain meteorological phenomena, to the authors' best knowledge, very few publications are available in the literature that discuss the issue of aerodynamic influences due to sand particles in the air.

Nowadays, computational fluid dynamics can solve complex flow problems, such as an air–sand particle two-phase flow problem. Additional transport equations for the secondary phase are solved using the CFD code and the interaction terms by which the mass, momentum, and energy exchanges between the phases can be handled.

For several years, great effort has been devoted to the study of the aerodynamic performance of wind turbine airfoils in air flow. One of the first examples of CFD calculations of the aerodynamic characteristics of an S809 airfoil was presented by Wolfe and Ochs [1]. In particular, Wolfe and Ochs [1] studied a steady-state laminar flow over an S809 airfoil using the commercial code CFD-ACE [2].

By comparing the computed pressure and aerodynamic coefficients with wind tunnel data from Delft University, it was revealed that the transition point from laminar to turbulent flow should be correctly modeled to ensure that the simulations for attached flow are accurate, and that the standard  $k-\epsilon$  turbulence model is not suitable at angles of attack with flow separation.

In 2006, Gupta and Gordon Leishman [3] modified the Leishman–Beddoes dynamic stall model in order to represent the unsteady aerodynamic behavior of the S809 airfoil for wind turbine applications, and they found that there was a good agreement between the predictions and experimental data for various angle of attack time histories. The results obtained suggest that the Leishman–Beddoes model coupled with a lifting-line model is able to predict the unsteady behavior of airfoil sections in attached flow, light stall, and deep dynamic stall, with knowledge of the static stall characteristics.

Qu et al. [4] have demonstrated that the Reynolds number has a direct impact on the aerodynamic performance of a wind turbine airfoil. More specifically, numerical simulations and experiments were used to predict the two-dimensional flow over an NREL S809 airfoil, and it was observed that, at Reynolds numbers varying from  $1.5 \times 10^4$  to  $2 \times 10^5$ , both drag and lift coefficients experience great changes, while at Reynolds numbers from  $2 \times 10^5$  to  $5 \times 10^6$  the changes are smoother and very small.

Later, a numerical simulation of transition effect on the aerodynamic performance of an S809 airfoil was conducted by Zhong et al. [5]. First, they observed the lift and drag characteristics in multiple turbulence models, paying no attention to transition, and then they simulated the aerodynamic performance of an S809 airfoil in order to investigate the laminar-to-turbulence transition effect on the airfoil's aerodynamic characteristics and the flow separation near the trailing edge. It was observed that transition significantly influences the lift and drag characteristics, as well as the flow separation near the trailing edge.

In a recent paper Douvi and Margaritis [6] presented a comparison between the aerodynamic performance of NACA 0012 and NREL S809 wind turbine airfoils at various angles of attack and operating at different Reynolds numbers using CFD code. After validating the obtained computational results by comparing them with experimental data, they concluded that the realizable  $k-\omega$  turbulence model was the most appropriate to describe the aerodynamic performance of both airfoils. It was also found that the S809 airfoil was more advantageous compared to the NACA 0012 airfoil.

Several publications have also appeared in recent years documenting the impact of a two-phase flow over the aerodynamic behavior of airfoils. In 2010, Wan and Pan [7] investigated the degradation on aerodynamic performance of an airfoil due to heavy rain, using a discrete phase model in order to simulate the two-phase flow. Wan and Chou [8] reinvestigated the influence of heavy rain on the aerodynamic performance of a high lift airfoil by simulating the rain conditions with a discrete phase model combined with high lift devices' surface roughness effects. The results obtained by Wan and Pan [7] as well as by Wan and Chou [8] suggest that the degradation rate increases with the rain rate.

Next, Douvi and Margaritis [9] utilized a discrete phase model on a CFD code in order to predict not only the aerodynamic characteristics of a NACA 0012 wind turbine airfoil under raining conditions, but also the flow field over the airfoil. The results emerged were compared with reliable experimental data, and after a comparison between simulations in both dry and wet conditions was conducted, it was possible to conclude that rain causes a decrease of the lift coefficient and an increase of the drag.

Another solution is described by Wu and Cao [10], who numerically simulated the flow over a NACA 0012 airfoil in heavy rain via a two-way coupled Eulerian–Lagrangian development. The predicted aerodynamic force coefficients agree well with the experimental results, and it was found that there was, approximately, a  $3^\circ$  rain-induced increase in stall angle of attack. Wu and Cao [10] also found that the airfoil aerodynamic efficiency degradation in a heavy rain environment was due to an uneven water film caused by the loss of boundary momentum by raindrop splashback and the effective roughening of the airfoil surface.

In 2014, Ren et al. [11] published a paper in which they described a numerical study about the influence of rime ice conditions on a NREL S809 airfoil under various temperatures and liquid water contents, operating at a Reynolds number of  $Re = 1 \times 10^6$ . The numerical calculations accomplished

on the transition shear-stress transport (SST) turbulent model using Fluent and Lewice software under the same icing conditions. However, the researchers have arrived at the conclusion that there was not good agreement between the numerical results obtained with Lewice and the experiments.

Recently, Olivieri et al. [12] studied the behavior of small particles affected by the Basset history term force in an isotropic and homogeneous turbulent flow, utilizing an Eulerian-Lagrangian approach. It was shown that the small-scale clustering of inertial particles is reduced by the Basset history term, as well as that by consideration of the Basset history at a low Reynolds numbers there are significant changes on the balance of forces, which determine the instantaneous acceleration of the particles.

In a paper by Sardina et al. [13], a stochastic model was proposed, and direct numerical simulation and large eddy simulations (LES) were used, in order to study the constant growth of cloud droplets because of their condensation in turbulent clouds in a homogeneous isotropic turbulent flow. It was concluded that the size of the droplet distribution increases with time and also that, given enough time, every warm cloud would precipitate.

Next, the focus of De Marchis et al. [14] has been on the effect of the wall roughness on dilute wall-bounded turbulent flows, because of the interaction between inertial particles that influence the macroscopic behavior of such two-phase systems, and coherent turbulent structures characteristic of the wall region. They used DNS at friction Reynolds number  $Re_\tau = 180$  combined with Lagrangian heavy particle tracking in a turbulent channel flow in order to characterize the effect of inertia on particle preferential accumulation.

However, to the authors' best knowledge, very few publications are available in the literature that discuss the issue of the impact of an air-sand particle two-phase flow on the aerodynamic performance of an airfoil. An interesting approach to this issue has been proposed by Khakpour et al. [15] in 2007, who studied the effect of sand particles on the flow over a S819 wind turbine airfoil and found that a greater particles mass flow rate results in a decrease of the pressure coefficient.

In 2009 Knopp et al. [16] presented an extension for  $k-\omega$  turbulence models, based on the equivalent sand grain approach, to account for wall roughness. Briefly, the grid requirements are the same for simulation of flows over both rough surfaces and smooth walls, the skin friction for transitional roughness Reynolds numbers prediction is improved and there is no need to modify the SST  $k-\omega$  model. Knopp et al. [16] indicate that this new method can be utilized to predict the aerodynamic effects of surface roughness on the flow past an airfoil in high lift conditions.

Salem et al. [17] have proposed a computational fluid dynamics (CFD) model coupled with a deposition model using the full two-dimensional Navier–Stokes equations and the SST  $k-\omega$  turbulence model in order to assess the performance degradation of wind turbine NACA 63-215 airfoil operating in dusty regions. The developed model predictions were validated by being compared with existing experimental data and the flow separation was identified by the numerical results.

However, studies on the aerodynamic performance of a NREL S809 wind turbine airfoil in an air-sand particle two-phase flow are still lacking. Therefore, the aim of the present paper is to investigate the air-sand particle steady incompressible two-phase flow over a NREL S809 wind turbine airfoil at various angles of attack and operating at Reynolds numbers of  $Re = 1 \times 10^6$  and  $Re = 2 \times 10^6$ , using CFD code. The computational results are compared with reliable existing experimental data on air flow over an S809 airfoil, in order to find the impact of sand particles on lift and drag coefficients and, consequently, the aerodynamic performance of the airfoil.

## 2. Discrete Two-Phase Flow over an Airfoil

Air-sand particle two-phase flow can be characterized as a discrete phase flow, which can be investigated computationally by the help of the Euler-Lagrange approach. The continuum air phase interacts with the dispersed phase, which consists of sand particles, and mass, energy, and momentum of the dispersed phase are exchanged with the air phase. Especially for air-sand particle two-phase flow, there is only momentum transfer from the air to the particles.

Regarding the discrete air-sand particle two-phase flow over an airfoil, sand particles influence plenty of characteristics, such as the shear stress factor, the pressure gradient, and the boundary layer and, as a result, the aerodynamic performance of the airfoil. More specifically, the lift force, in other words the component of the net affecting force on the airfoil acting normal to the incoming flow stream decreases, while the drag force, which is the component of the net force acting parallel to the incoming flow stream, increases due to the change in momentum caused by the reflected particles, as they impact the airfoil.

### 3. Computational Method

#### 3.1. Computational Mesh

First of all, before the numerical study, the NREL S809 wind turbine airfoil profile was imported to the geometry system. Notably, the S809 is a 21% thick, laminar-flow airfoil, designed specifically for HAWT applications by Somers [18]. In 1980, the S809 profile was developed using the Eppler design code by Eppler and Somers [19,20].

Second, the meshes, as well as the boundary conditions, were created in the mesh component system, where two-dimensional and three-dimensional models can be produced using structured or unstructured meshes consisting of a variety of quadrilateral, triangular, or tetrahedral elements. The mesh is denser in regions where greater computational accuracy is needed, namely in the region close to the airfoil. These applications can be accessed from ANSYS Workbench, which combines access to ANSYS applications with utilities that manage the product workflow.

Next, it was necessary to choose the most appropriate structured mesh; in other words, to conduct a grid independence study. In general, as more nodes are used, the more accurate the numerical solution becomes. However, utilizing additional nodes results in an increase of the required computer memory, as well as an increase of the computational time. Increasing the number of nodes until the mesh is sufficiently fine, so that further refinement does not change the results, can determine the appropriate number of nodes needed.

After the conduction of the grid independence study, a C-type grid topology consisted of 80,000 quadrilateral cells was shown to be the most appropriate for a grid independent solution for an S809 airfoil; the domain height was set to 25 chord lengths, while the height of the first cell adjacent to the surface was set to  $10^{-5}$ , corresponding to a maximum  $y^+$  of approximately 0.2, a sufficient size to properly resolve the inner parts of the boundary layer. The C-type grid and the detail of the mesh close to the S809 airfoil are presented in Figure 1.

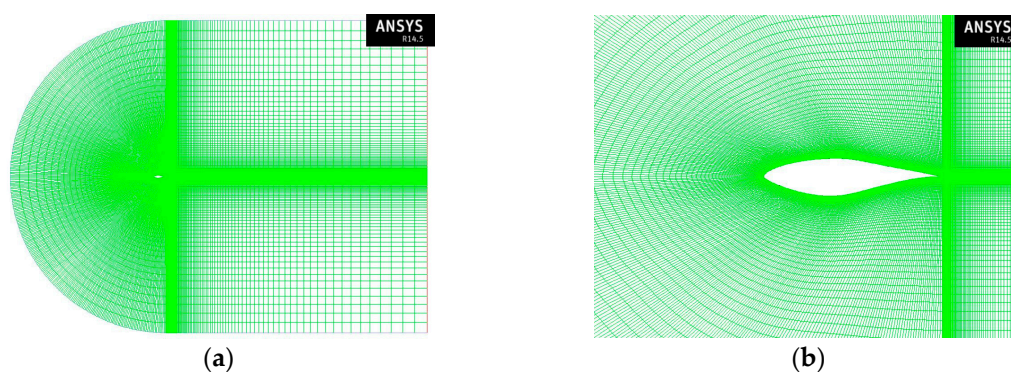


**Figure 1.** (a) C-type grid with 80,000 quadrilateral cells; and (b) detail of the mesh close to the S809 airfoil.

### 3.2. Turbulence Models

The utilized segregated, implicit solver, ANSYS Fluent 14.5 [21], solves conservation equations for mass and momentum for all flows, as well as additional transport equations if the flow is turbulent. In the current study, the simulation of the air-sand particle steady incompressible two-phase flow over the airfoil is accomplished via an Euler-Lagrange approach in ANSYS Fluent, the Lagrangian discrete phase model (DPM). The continuum air phase is solved by the Navier–Stokes equations, while the dispersed phase, consisted of a large number of spherical sand particles, is solved by tracking them through the calculated flow field.

Given the viscosity of the fluid,  $\mu$ , the drag coefficient,  $C_D$ , the relative Reynolds number,  $Re$ , the density of the particle,  $\rho_p$ , the diameter of the particle,  $d_p$ , the velocity of the particle,  $u_p$ , the velocity of the fluid,  $u$ , the mass flow rate of the particles,  $\dot{m}_p$ , the time step,  $\Delta t$ , and other interaction forces,  $F_{other}$ , the change in momentum of a sand particle through each control volume can be calculated by the following equation:

$$F = \sum \left( \frac{18\mu C_D Re}{\rho_p d_p^2 24} (u_p - u) + F_{other} \right) \dot{m}_p \Delta t \quad (1)$$

The integration of the force balance on the particle predicts the trajectory of a discrete phase particle. The force balance is written in a Lagrangian reference frame. The forces acting on the particle are equal to the particle inertia and, particularly in the  $x$  direction, this equality can be expressed as:

$$\frac{du_p}{dt} = F_D (\vec{u} - \vec{u}_p) + \frac{\vec{g}}{\rho_p} (\rho_p - \rho) + \vec{F} \quad (2)$$

where:

$$F_D = \frac{18\mu C_D Re}{\rho_p d_p^2 24} \quad (3)$$

where  $F_D (\vec{u} - \vec{u}_p)$  is the drag force per unit particle mass and  $\vec{F}$  is an additional acceleration term, also the force per unit particle mass.

In the above equations  $\vec{u}_p$  is the particle velocity,  $\vec{u}$  is the fluid phase velocity,  $\rho_p$  is the density of the particle,  $\rho$  is the fluid density,  $\mu$  is the molecular viscosity of the fluid,  $d_p$  is the particle diameter and  $Re$  is the relative Reynolds number, which is defined as:

$$Re \equiv \frac{\rho d_p |\vec{u}_p - \vec{u}|}{\mu} \quad (4)$$

The flow behavior is turbulent; therefore, the numerical simulations were accomplished on realizable  $k-\epsilon$  and SST  $k-\omega$  turbulence models, which are appropriate for aerodynamic applications. This section outlines these two turbulence models. In the two-phase flow, because of particles damping and production of turbulence eddies, two-way turbulence coupling is enabled in order to consider the effect of particles' existence in turbulent quantities.

The realizable  $k-\epsilon$  model proposed by Shih et al. [22] is one of the simplest turbulence complete models that consists of two equations. In the realizable  $k-\epsilon$  model, two separate transport equations are solved and the turbulent velocity and length scales can be determined independently. The term “realizable” implies that certain mathematical restrictions on the Reynolds stresses, which are consistent with the physics of turbulent flows, are satisfied. Notably, the realizable  $k-\epsilon$  model contains a new eddy-viscosity formula involving a variable  $c_\mu$  originally proposed by Reynolds [23] and a new model equation for dissipation ( $\epsilon$ ) based on the dynamic equation of the mean-square vorticity fluctuation.

Next, Menter [24] developed the shear-stress transport (SST)  $k-\omega$  model in order to combine effectively the robust and exact formulation of the  $k-\omega$  model in the near-wall region with the free-stream independence of the  $k-\epsilon$  model in the far field, by converting the  $k-\epsilon$  model into a  $k-\omega$

formulation. The SST  $k-\omega$  model includes some refinements, which make it more accurate and reliable for a wider class of flows, such as adverse pressure gradient flows, airfoils, and transonic shock waves, than the standard  $k-\omega$  model.

The numerical simulations were accomplished using ANSYS Fluent 14.5 [21] and calculations were made for angles of attack ranging from  $-9^\circ$  to  $16^\circ$  for two different concentrations of sand particles in the air flow, more specifically 1% and 10%, while the diameter of sand particles was chosen to be 0.5 mm and the density  $2196.06 \text{ kg/m}^3$ . Regarding the Reynolds numbers for the simulation, they were chosen to be  $Re = 1 \times 10^6$  and  $Re = 2 \times 10^6$ , in order to be validated in the present simulations by being compared to reliable experimental data regarding the air flow over the airfoil. Moreover, the flow can be described as incompressible, an assumption close to reality, so it is not necessary to solve the energy equation. The free stream temperature was chosen to be same as the environmental temperature, in other words, equal to 300 K. Subsequently, the density of the air is  $\rho = 1.225 \text{ kg/m}^3$  and the viscosity is  $\mu = 1.7894 \times 10^{-5} \text{ kg/ms}$ .

Notably, the sand particles are tracked at the minimum distance upstream of the airfoil where the flow is undisturbed as to simplify the solution and to reduce the computational time. Figure 2 illustrates the distance upstream of the airfoil where the particles are tracked. The horizontal axis velocity is chosen to be equal to air velocity, while the vertical axis velocity is calculated by the approach method and depends on the diameter of the sand particles.

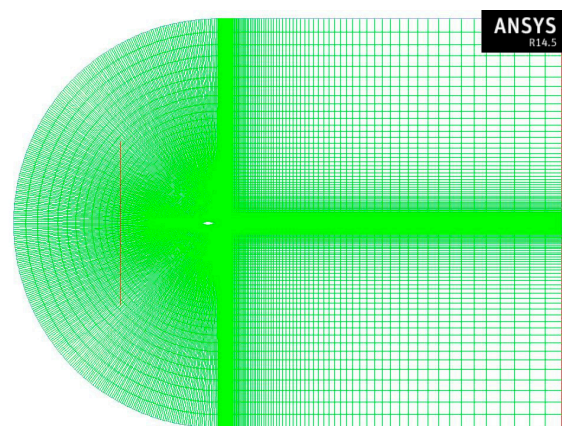


**Figure 2.** The minimum distance upstream of the airfoil where the particles are tracked.

#### 4. Results and Discussion

Numerical simulations were conducted at various angles of attack and at Reynolds numbers of  $Re = 1 \times 10^6$  and  $Re = 2 \times 10^6$ . The component of the net affecting force on the airfoil acting normal to the incoming flow stream is known as the lift force, while the component of the net force acting parallel to the incoming flow stream is known as the drag force. The lift and drag coefficients were possible to be predicted by means of the realizable  $k-\epsilon$  and SST  $k-\omega$  turbulence models, and then to be examined and compared with reliable experimental data regarding the one-phase air flow over the S809 airfoil by Somers [18].

Figures 3 and 4 illustrate the simulation results of the lift coefficient for the S809 airfoil versus the angle of attack at Reynolds numbers of  $Re = 1 \times 10^6$  and  $Re = 2 \times 10^6$ , respectively, for one-phase flow and two-phase flows of two different concentrations of sand particles in the air. Regarding the numerical results for the one phase air flow, it is obvious that the lift coefficient increases linearly with the angle of attack in the range of  $-9^\circ$  to  $9^\circ$ . The turbulence models are shown to have the same behavior and good agreement with the experimental data. Nevertheless, for angles of attack higher than  $12^\circ$ , there is a disagreement between the experimental data and the computational results. Furthermore, it can be observed that sand concentration affects the lift coefficients. More specifically, there is a downward translation of the lift coefficient curve as the concentrations of sand particles

increase, which has, as a result, a degradation of the aerodynamic performance. This degradation increases as the angle of attack and the concentration of sand particles increase.

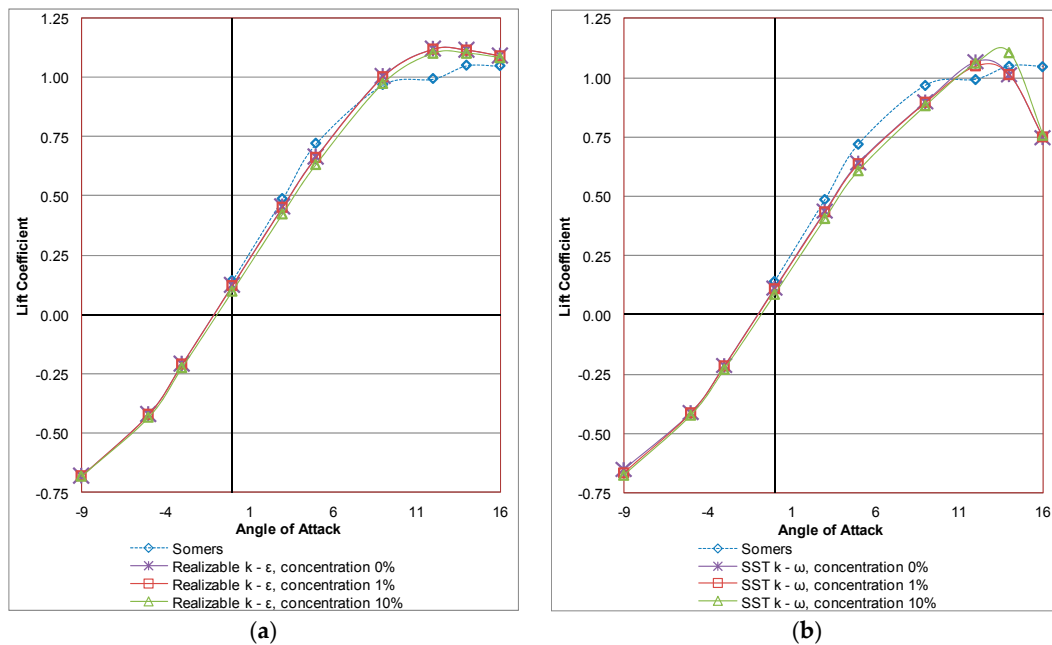


**Figure 3.** Comparison between reliable experimental data and simulation results of the lift coefficient curve for an S809 airfoil for (a) realizable  $k-\epsilon$ ; and (b) SST  $k-\omega$  turbulence models at  $Re = 1 \times 10^6$  for one-phase and two-phase flows consisting of two different concentrations of sand particles in the air.

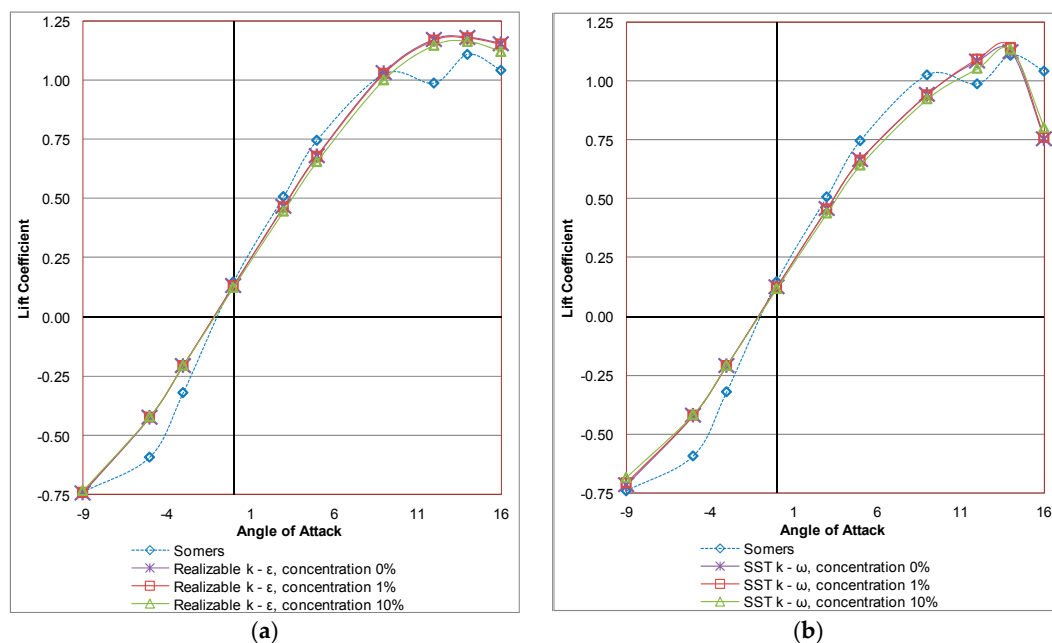


**Figure 4.** Comparison between reliable experimental data and simulation results of the lift coefficient curve for an S809 airfoil for (a) realizable  $k-\epsilon$ ; and (b) SST  $k-\omega$  turbulence models at  $Re = 2 \times 10^6$  for one-phase and two-phase flows consisting of two different concentrations of sand particles in the air.

Figures 5 and 6 depict the simulation results of the drag coefficient for the S809 airfoil versus the angle of attack at  $Re = 1 \times 10^6$  and  $Re = 2 \times 10^6$ , respectively. For both Reynolds numbers the predicted drag coefficient increases as the angle of attack and the concentrations of sand particles in

the air increase. This increase is much more obvious for 10% concentration of sand particles in the air flow. The larger total drag is caused by the mixture of air and sand particles, which results in larger skin frictional drag. Despite that there is a significant difference between experimental data and numerical results.

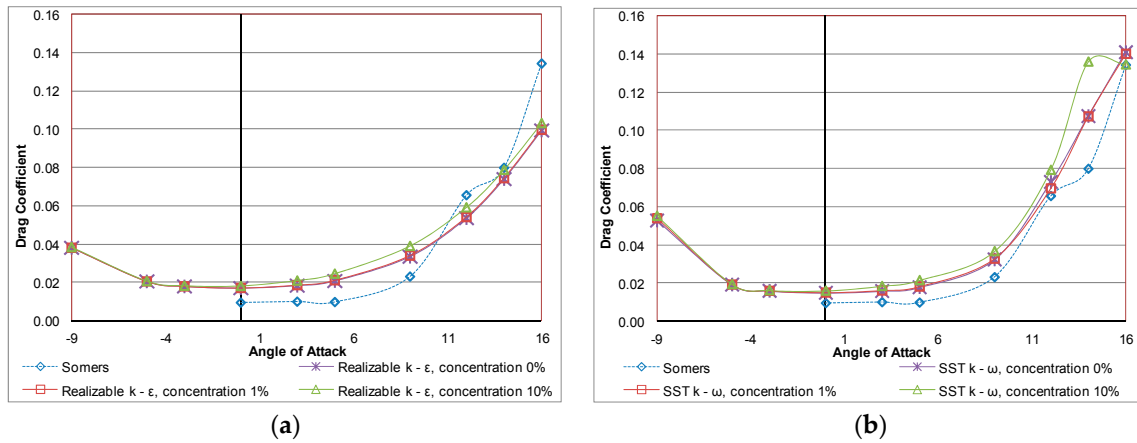


**Figure 5.** Comparison between reliable experimental data and simulation results of the drag coefficient curve for an S809 airfoil for (a) realizable  $k-\epsilon$ ; and (b) SST  $k-\omega$  turbulence models at  $Re = 1 \times 10^6$  for one-phase and two-phase flows consisting of two different concentrations of sand particles in the air.

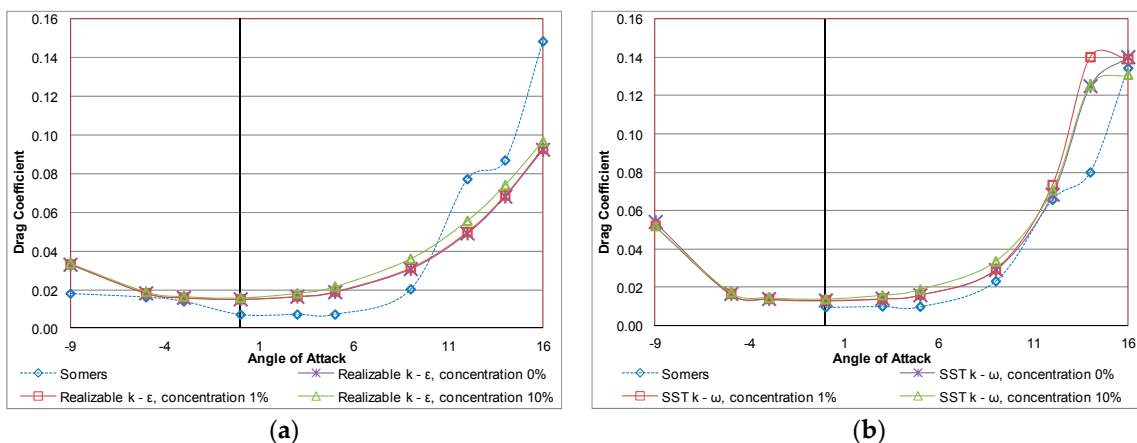


**Figure 6.** Comparison between reliable experimental data and simulation results of the drag coefficient curve for an S809 airfoil for (a) realizable  $k-\epsilon$ ; and (b) SST  $k-\omega$  turbulence models at  $Re = 2 \times 10^6$  for one-phase and two-phase flows consisting of two different concentrations of sand particles in the air.

As follows from the figures shown above, it can be concluded that the realizable  $k-\epsilon$  turbulence model seems to be more appropriate than SST  $k-\omega$  model to describe the two-phase flow over the S809 airfoil since the effect of sand concentration on the aerodynamic performance of the airfoil is more obvious for a wider range of angles of attack.

Next, Figures 7–12 present the region around the S809 airfoil using contours of static pressure at angles of attack equal to  $-3^\circ$ ,  $0^\circ$ ,  $3^\circ$ , and  $9^\circ$ , and at Reynolds numbers of  $Re = 1 \times 10^6$  and  $Re = 2 \times 10^6$  with the realizable  $k-\epsilon$  model for air flow and air-sand particle two-phase flow consisting of 1% and 10% concentration of sand particles in the air.

To begin with, Figure 7 shows the contours of static pressure at various angles of attack and at  $Re = 1 \times 10^6$  for an S809 airfoil for air flow. Notably, the stagnation points, in other words the points in a flow where the fluid velocity is zero and, thus, the static pressure is equal to the total, are obvious. As can be seen, the pressure on the lower- $\epsilon$  surface of the airfoil is greater than the pressure of the

incoming flow stream. As a result, the airfoil is effectively “pushed” upward, normal to the incoming flow stream. Moreover, it can be seen that as the angle of attack increases, the trailing edge stagnation point moves forward on the airfoil.

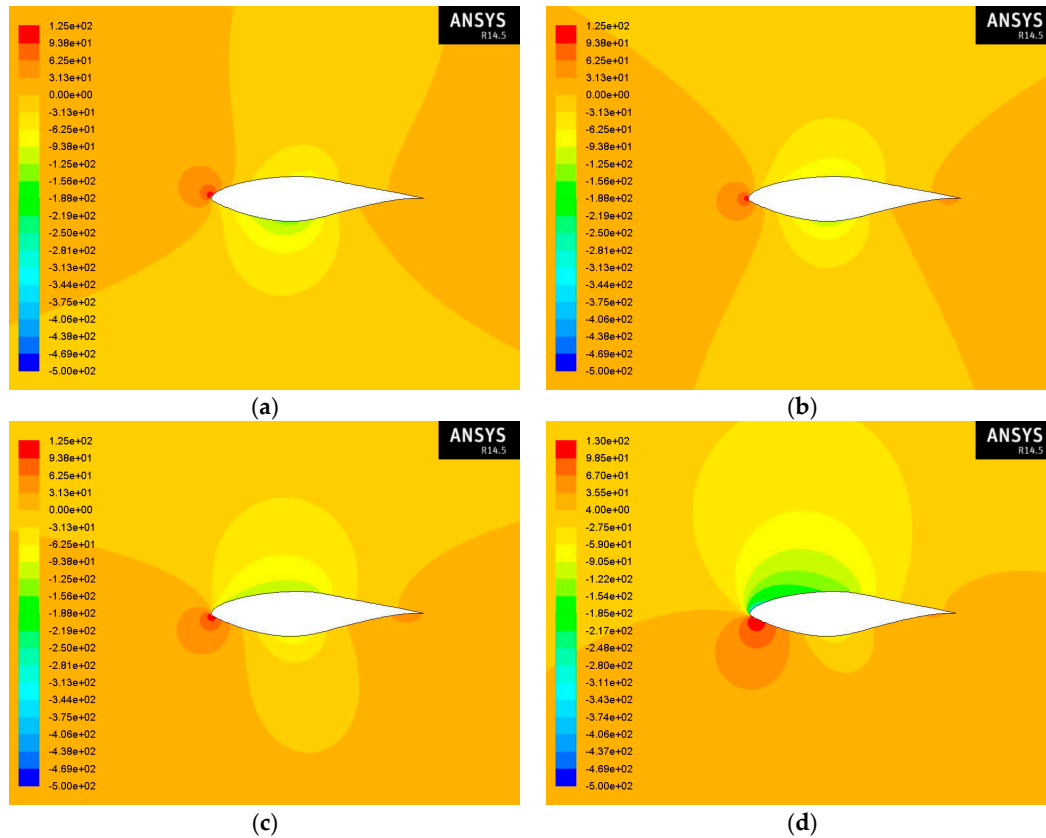


**Figure 7.** Contours of static pressure at (a)  $-3^\circ$ ; (b)  $0^\circ$ ; (c)  $3^\circ$ ; and (d)  $9^\circ$  angles of attack at  $Re = 1 \times 10^6$  with the realizable  $k-\epsilon$  turbulence model for an S809 airfoil for air flow.

Regarding the effect of sand particles on the aerodynamic performance, the contours shown in Figure 8 in the case of 1% concentration of sand particles in the air seem to be almost the same with the respective static pressure contours for the air flow.

In Figure 9 are shown the contours of static pressure in the case of 10% concentration of sand particles in the air. In comparison with the contours for the air flow a very small difference can be observed. More specifically, the pressure seems to achieve lower values on the lower surface and higher values on the upper surface as the concentration increases.

The contours of static pressure at various angles of attack and at  $Re = 2 \times 10^6$  for air flow and air-sand particle two-phase flow for 1% and 10% concentration of sand particles in the air are given in Figures 10–12 and they seem to have similar behavior with the contours of static pressure at  $Re = 1 \times 10^6$ . However, as the Reynolds number increases, the upper surface pressure achieves lower values for each angle of attack.

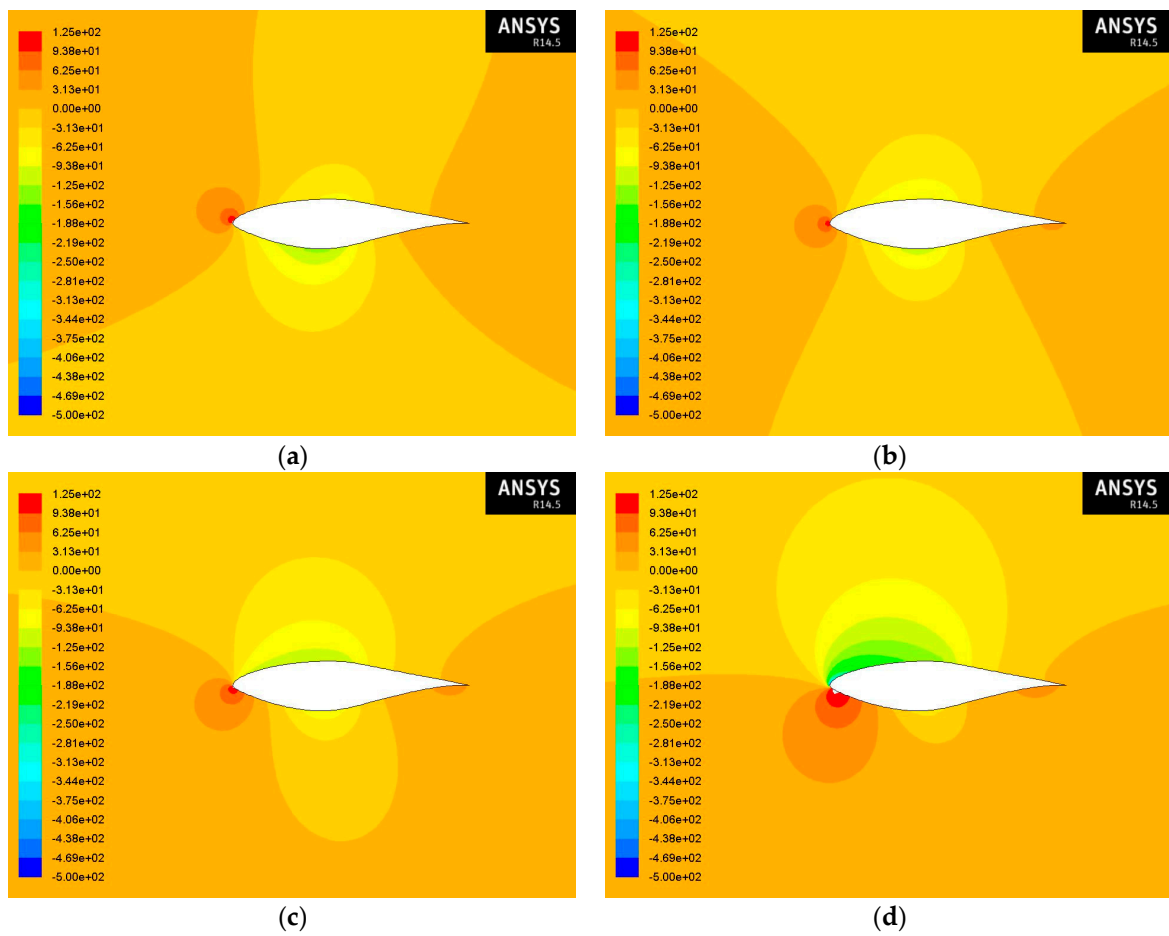


**Figure 8.** Contours of static pressure at (a)  $-3^\circ$ ; (b)  $0^\circ$ ; (c)  $3^\circ$ ; and (d)  $9^\circ$  angles of attack at  $Re = 1 \times 10^6$  with the realizable  $k-\epsilon$  turbulence model for an S809 airfoil for air-sand particle two-phase flow and 1% concentration of sand particles in the air.

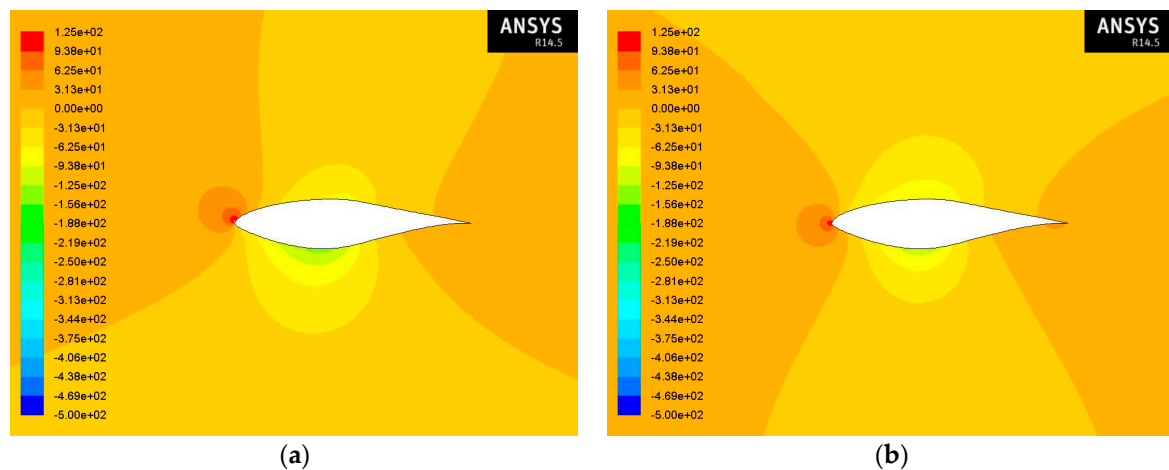


**Figure 9.** Cont.

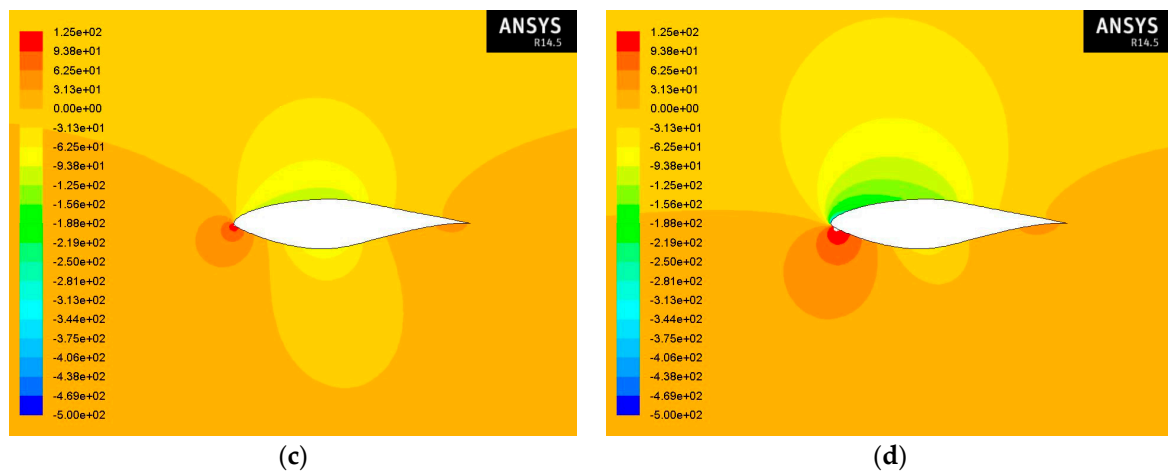


**Figure 9.** Contours of static pressure at (a)  $-3^\circ$ ; (b)  $0^\circ$ ; (c)  $3^\circ$ ; and (d)  $9^\circ$  angles of attack at  $Re = 1 \times 10^6$  with the realizable  $k-\epsilon$  turbulence model for and S809 airfoil for air-sand particle two-phase flow and 10% concentration of sand particles in the air.

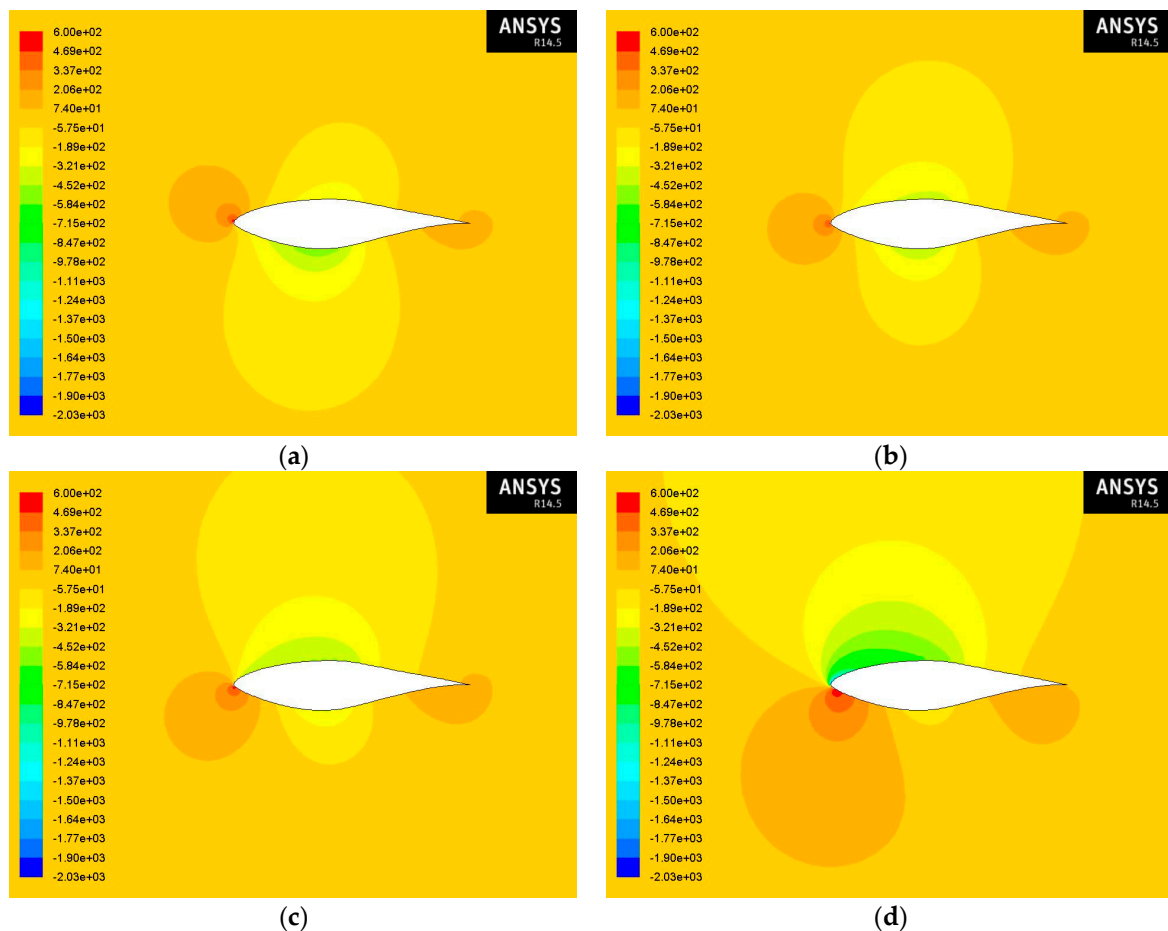


**Figure 10.** Contours of static pressure at (a)  $-3^\circ$ ; (b)  $0^\circ$ ; (c)  $3^\circ$ ; and (d)  $9^\circ$  angles of attack at  $Re = 2 \times 10^6$  with the realizable  $k-\epsilon$  turbulence model for an S809 airfoil for air flow.

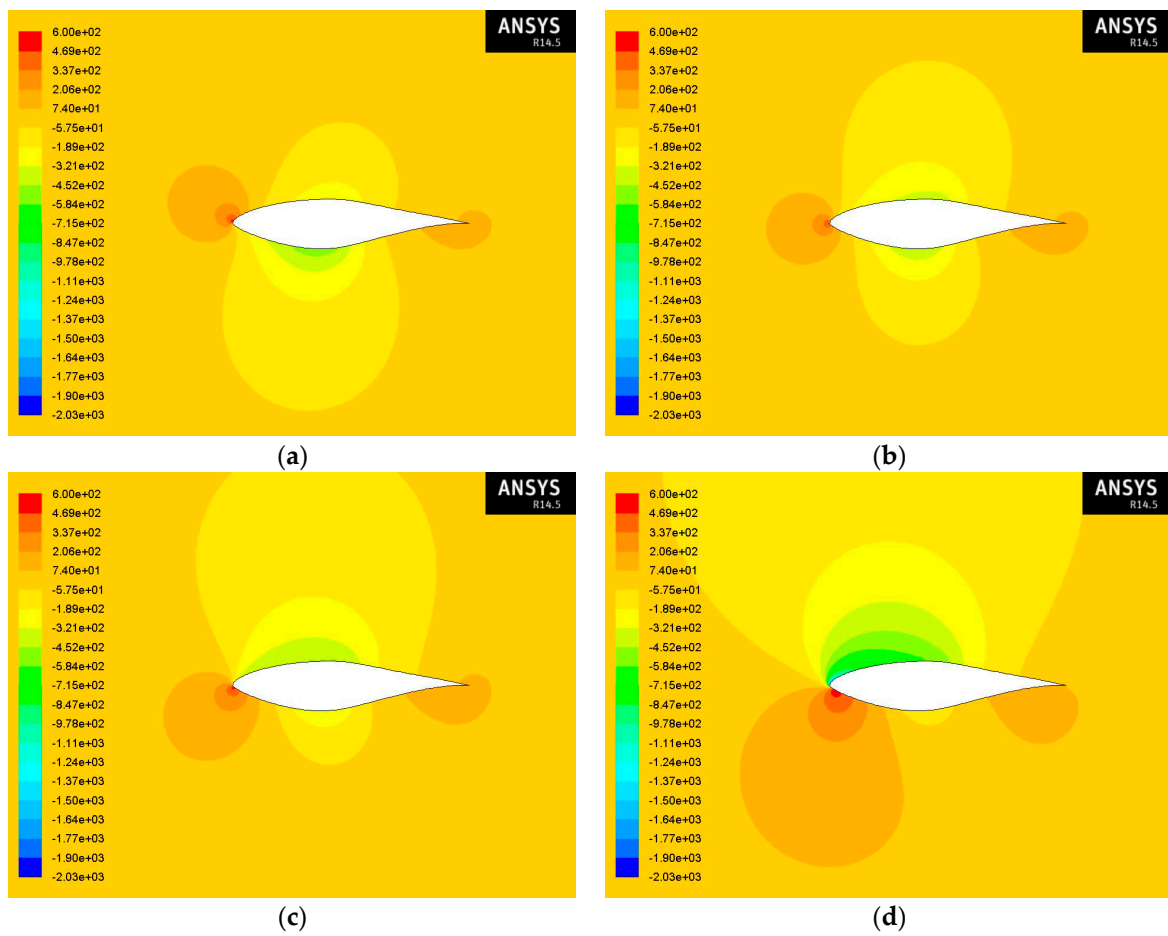


**Figure 11.** Contours of static pressure at (a)  $-3^\circ$ ; (b)  $0^\circ$ ; (c)  $3^\circ$ ; and (d)  $9^\circ$  angles of attack at  $Re = 2 \times 10^6$  with the realizable  $k-\epsilon$  turbulence model for an S809 airfoil for air-sand particle two-phase flow and 1% concentration of sand particles in the air.

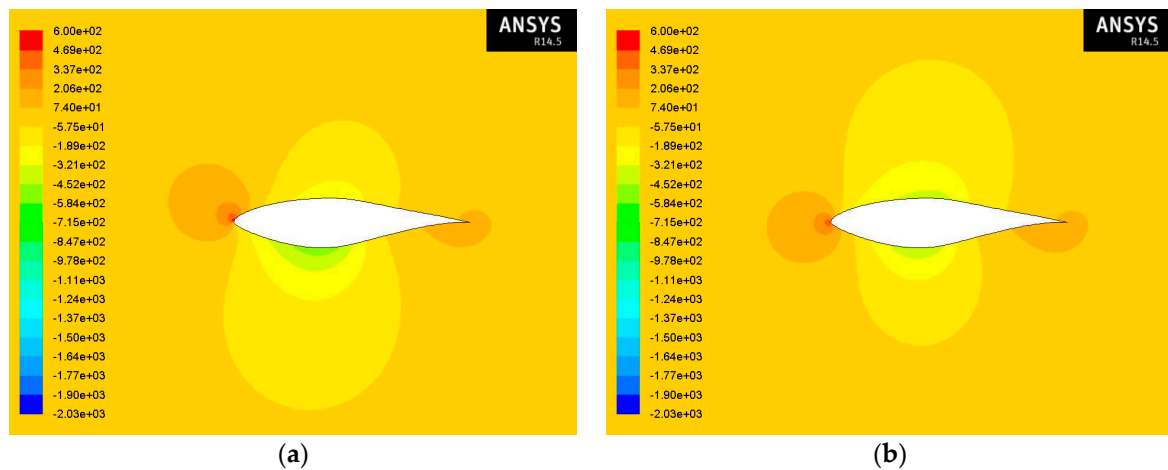


**Figure 12.** Cont.

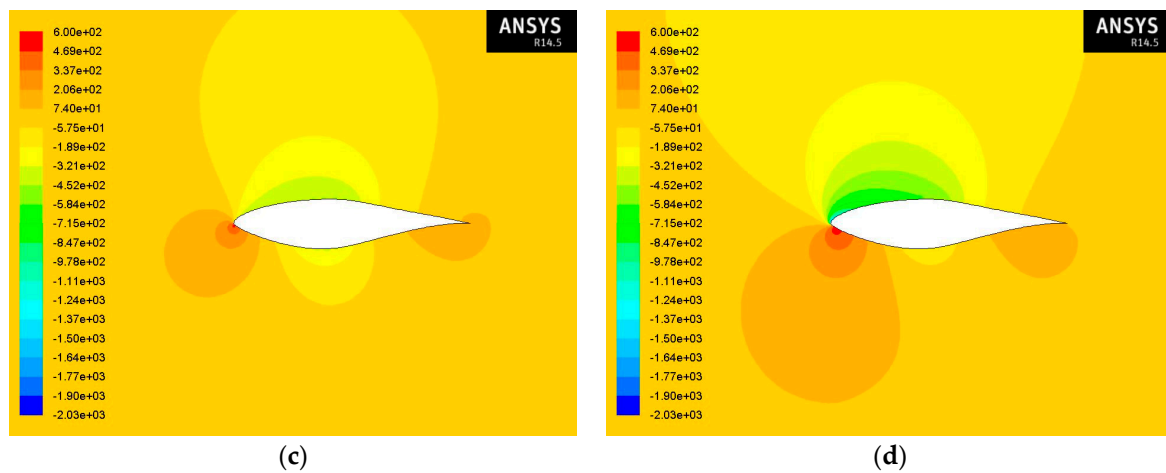


**Figure 12.** Contours of static pressure at (a)  $-3^\circ$ ; (b)  $0^\circ$ ; (c)  $3^\circ$ ; and (d)  $9^\circ$  angles of attack at  $Re = 2 \times 10^6$  with the realizable  $k-\epsilon$  turbulence model for an S809 airfoil for air-sand particle two-phase flow and 10% concentration of sand particles in the air.

Subsequently, Figures 13 and 14 provide the contours of sand particle concentration over the S809 airfoil at various angles of attack and at  $Re = 1 \times 10^6$  for 1% and 10% concentration of sand particles in the air, respectively, with the realizable  $k-\epsilon$  turbulence model. As can be seen, the sand particles tend to concentrate mainly in the region of the trailing edge to the middle of the airfoil, and as the concentration of them in the air increases, the airfoil is surrounded by more particles.

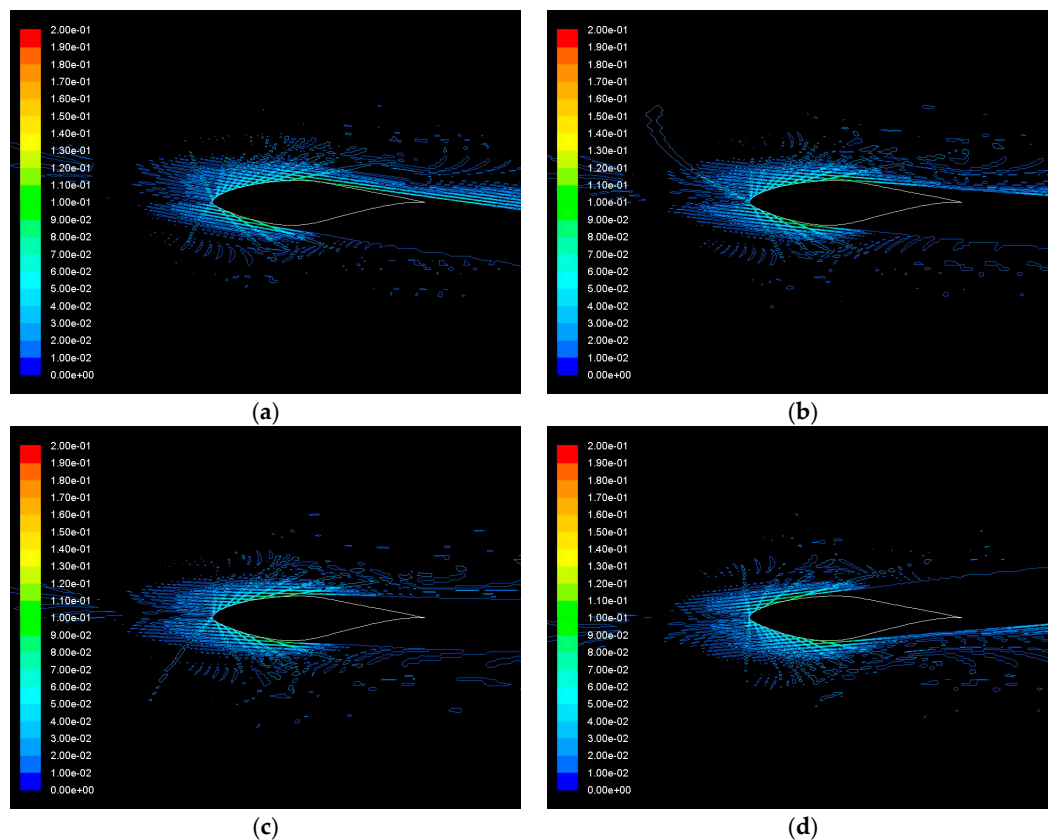


**Figure 13.** Contours of DPM concentration at (a)  $-3^\circ$ ; (b)  $0^\circ$ ; (c)  $3^\circ$ ; and (d)  $9^\circ$  angles of attack at  $Re = 1 \times 10^6$  with the realizable  $k-\epsilon$  turbulence model for an S809 airfoil for air-sand particle two-phase flow and 1% concentration of sand particles in the air.

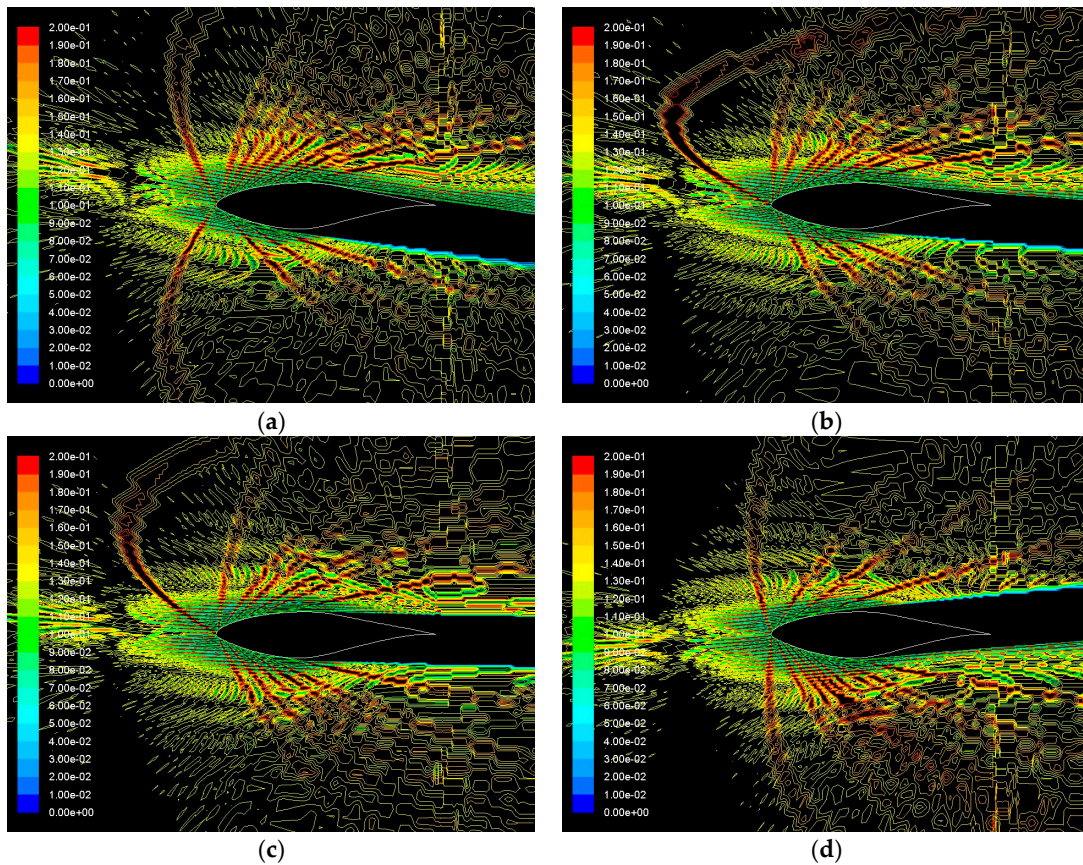


**Figure 14.** Contours of DPM concentration at (a)  $-3^\circ$ ; (b)  $0^\circ$ ; (c)  $3^\circ$ ; and (d)  $9^\circ$  angles of attack at  $Re = 1 \times 10^6$  with the realizable  $k-\epsilon$  turbulence model for an S809 airfoil for air-sand particle two-phase flow and 10% concentration of sand particles in the air.

Similarly, regarding the contours of sand particles concentration over the S809 airfoil at a Reynolds number of  $Re = 2 \times 10^6$  with the realizable  $k-\epsilon$  turbulence model for 1% concentration of sand particles in the air as shown in Figure 15, and 10% concentration of sand particles in the air as illustrated in Figure 16, the sand particles seem to have the same behavior as the concentration of them in the air increases, as for the case of  $Re = 1 \times 10^6$ . Furthermore, it can be observed that, as the Reynolds number increases, the sand particles drift towards the trailing edge of the airfoil.

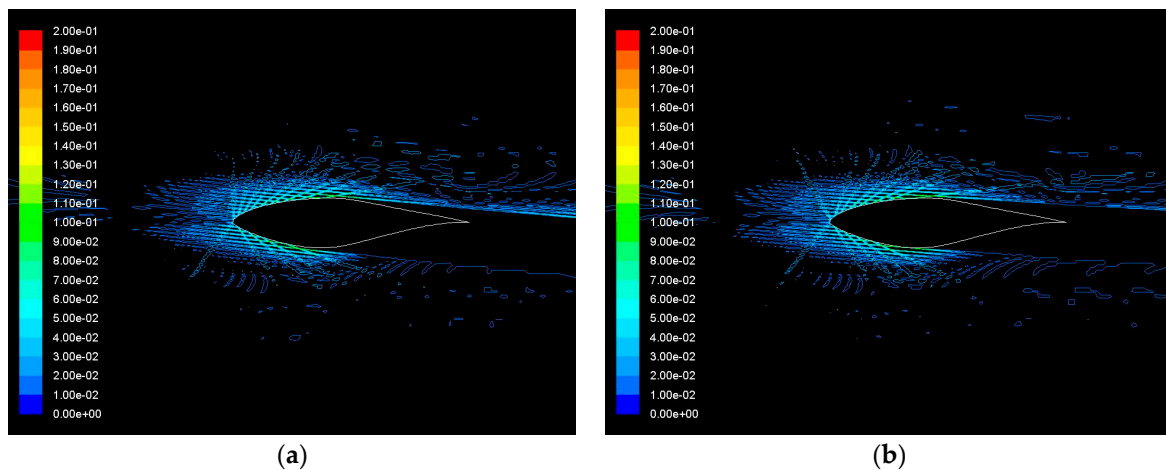


**Figure 15.** Cont.

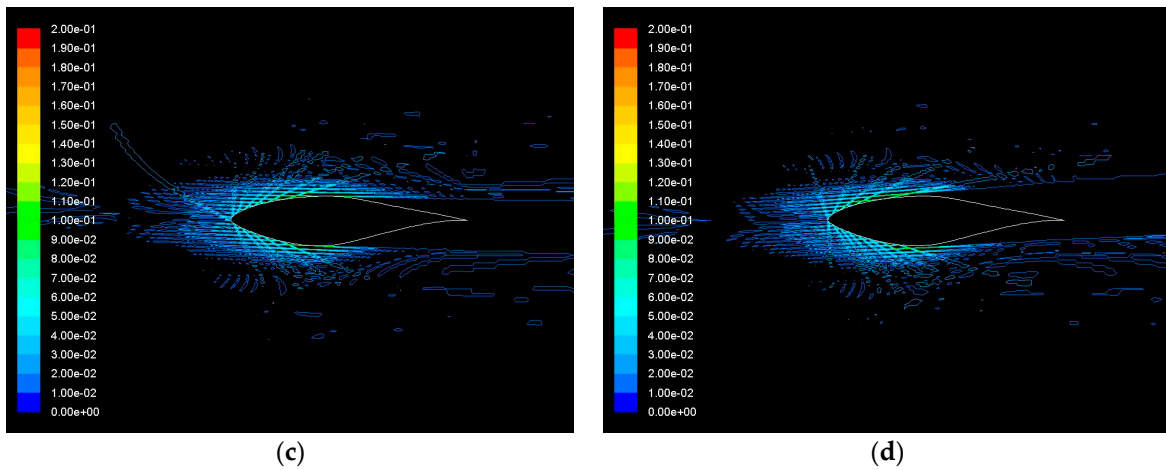


**Figure 15.** Contours of DPM concentration at (a)  $-3^\circ$ ; (b)  $0^\circ$ ; (c)  $3^\circ$ ; and (d)  $9^\circ$  angles of attack at  $Re = 2 \times 10^6$  with the realizable  $k-\epsilon$  turbulence model for an S809 airfoil for air-sand particle two-phase flow and 1% concentration of sand particles in the air.

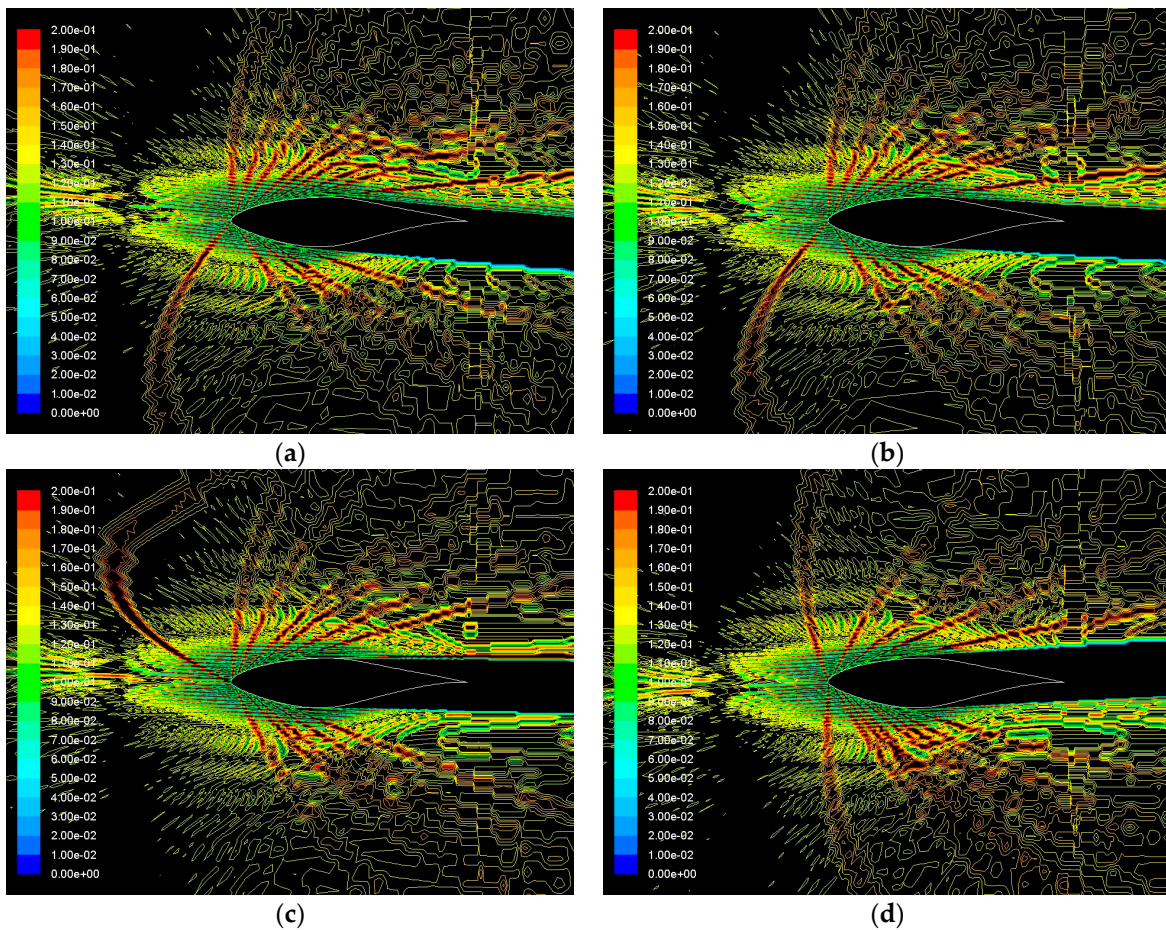


**Figure 16.** Contours of DPM concentration at (a)  $-3^\circ$ ; (b)  $0^\circ$ ; (c)  $3^\circ$ ; and (d)  $9^\circ$  angles of attack at  $Re = 2 \times 10^6$  with the realizable  $k-\epsilon$  turbulence model for an S809 airfoil for air-sand particle two-phase flow and 10% concentration of sand particles in the air.

## 5. Conclusions

The present study set out to determine the effect of air-sand particle two-phase flow, consisting of two different concentrations of sand particles in the air, on the aerodynamic performance of an S809 airfoil at Reynolds numbers of  $Re = 1 \times 10^6$  and  $Re = 2 \times 10^6$ .

Summing up the results, it can be concluded that the aerodynamic performance of the S809 airfoil degrades in the two-phase flow; in other words, the lift coefficient decreases and, simultaneously, the drag coefficient increases. In general, the degradation increases as the angle of attack and the concentration of sand particles increase for both Reynolds numbers. The mixture of air and sand particles change the skin friction to greater values and, thus, the total drag is larger.

From the outcome of the current investigation it is also possible to conclude that the realizable  $k-\epsilon$  model seems to be the most appropriate turbulence model to predict the degradation of the aerodynamic performance of a S809 airfoil due to the concentration of sand particles in the air flow at a wide range of angles of attack.

Moreover, based on the illustration of the flow field around the S809 airfoil, our understanding of the effects of sand concentration in air can be enhanced. It has been shown that the static pressure in the case of a 1% concentration of sand is almost the same with the pressure in the air flow, while in the case of a 10% concentration, a very small difference can be observed. It is apparent that the lower surface of the airfoil seems to have lower values, and the upper surface higher values, of static pressure as the sand concentration increases for both Reynolds numbers.

Finally, the contours of sand particle concentration over the S809 airfoil suggests that, in general, the sand particles tend to concentrate mainly in the region of the trailing edge to the middle of the airfoil, and as the concentration of them in the air increases, the airfoil is surrounded by more particles. Additionally, the particles drift towards the trailing edge of the airfoil by increasing the Reynolds number.

**Author Contributions:** Dimitra C. Douvi performed the simulations for Reynolds number of  $Re = 2 \times 10^6$  and wrote the paper; Dimitra C. Douvi and Dionissios P. Margaris analyzed the data; Aristeidis E. Davaris performed the simulations for Reynolds number of  $Re = 1 \times 10^6$ .

**Conflicts of Interest:** The authors declare no conflict of interest.

## References

1. Wolfe, W.P.; Ochs, S.S. CFD Calculations of S809 Aerodynamic Characteristics. In Proceedings of the 35th Aerospace Sciences Meeting and Exhibit, AIAA, Reno, NV, USA, 6–9 January 1997.
2. CFD Research Corporation. *CFD-ACE, Theory Manual*; Version 1.0; CFD Research Corporation: Huntsville, AL, USA, 1993.
3. Gupta, S.; Leishman, J.G. Dynamic Stall Modeling of the S809 Airfoil and Comparison with Experiments. In Proceedings of the Collection of Technical Papers—44th AIAA Aerospace Sciences Meeting, Reno, NV, USA, 9–12 January 2006.
4. Qu, H.; Hu, J.; Gao, X. The Impact of Reynolds Number on Two-Dimensional Aerodynamic Airfoil Flow. In Proceedings of the 2009 World Non-Grid-Connected Wind Power and Energy Conference, WNWEC 2009, Nanjing, China, 24–26 September 2009.
5. Zhong, W.; Wang, T.; Wang, Q. Numerical Simulation of Transition Effect on Aerodynamic Performance of Aerofoil S809. *Taiyangneng Xuebao/Acta Energeticae Sol. Sin.* **2011**, *32*, 1523–1527. (In Chinese)
6. Douvi, D.C.; Margaris, D.P. Comparison Between New and Existing Turbulence Models for Numerical Simulation of the Flow Over NACA 0012 and S809 Airfoils for Two Reynolds Numbers. In Proceedings of the 6th International Conference on “Experiments/Process/System Modelling/Simulation/Optimization”, Athens, Greece, 8–11 July 2015.
7. Wan, T.; Pan, S.-P. Aerodynamic efficiency study under the influence of heavy rain via Two-Phase Flow Approach. In Proceedings of the 27th Congress of the International Council of the Aeronautical Sciences 2010, ICAS 2010, Cancun, Mexico, 7–13 March 2010.

8. Wan, T.; Chou, C.-J. Reinvestigation of High Lift Airfoil under the Influence of Heavy Rain Effects. In Proceedings of the 50th AIAA Aerospace Sciences Meeting Including the New Horizons Forum and Aerospace Exposition, Nashville, Tennessee, 9–12 January 2012.
9. Douvi, E.C.; Margaris, D.P. Aerodynamic performance investigation under the influence of heavy rain of a NACA 0012 airfoil for wind turbine applications. *Int. Rev. Mech. Eng.* **2012**, *6*, 1228–1235.
10. Wu, Z.; Cao, Y. Numerical Simulation of Flow over an Airfoil in Heavy Rain via a Two-Way Coupled Eulerian-Lagrangian Approach. *Int. J. Multiph. Flow* **2015**, *69*, 81–92. [[CrossRef](#)]
11. Ren, P.-F.; Xu, Y.; Song, J.-J.; Xu, J.-Z. Numerical Study about the Influence of Rime Ice Conditions on Airfoil. *Kung Cheng Je Wu Li Hsueh Pao/J. Eng. Thermophys.* **2014**, *35*, 663–668.
12. Olivieri, S.; Picano, F.; Sardina, G.; Iudicone, D.; Brandt, L. The effect of the Basset history force on particle clustering in homogeneous and isotropic turbulence. *Phys. Fluids* **2014**, *26*, 041704. [[CrossRef](#)]
13. Sardina, G.; Picano, F.; Brandt, L.; Caballero, R. Continuous Growth of Droplet Size Variance due to Condensation in Turbulent Clouds. *Phys. Rev. Lett.* **2015**, *115*, 184501. [[CrossRef](#)] [[PubMed](#)]
14. De Marchis, M.; Milici, B.; Sardina, G.; Napoli, E. Interaction between turbulent structures and particles in roughened channel. *Int. J. Multiph. Flow* **2016**, *78*, 117–131. [[CrossRef](#)]
15. Khakpour, Y.; Bardakji, S.; Nair, S. Aerodynamic Performance of Wind Turbine Blades in Dusty Environments. In Proceedings of the ASME 2007 International Mechanical Engineering Congress and Exposition, IMECE2008, Seattle, WA, USA, 11–15 November 2007.
16. Knopp, T.; Eisfeld, B.; Calvo, J.B. A New Extension for  $k-\omega$  Turbulence Models to Account for Wall Roughness. *Int. J. Heat Fluid Flow* **2009**, *30*, 54–65. [[CrossRef](#)]
17. Salem, H.; Diab, A.; Ghoneim, Z. CFD Simulation and Analysis of Performance Degradation of Wind Turbine Blades in Dusty Environments. In Proceedings of the 2013 International Conference on Renewable Energy Research and Applications, ICRERA 2013, Madrid, Spain, 20–23 October 2013.
18. Somers, D.M. *Design and Experimental Results for the S809 Airfoil*; National Renewable Energy Laboratory: Golden, CO, USA, 1997.
19. Eppler, R.; Somers, D.M. *A Computer Program for the Design and Analysis of Low-Speed Airfoils*; NASA: Hampton, VA, USA, 1980.
20. Eppler, R.; Somers, D.M. *Supplement to: A Computer Program for the Design and Analysis of Low-Speed Airfoils*; NASA: Hampton, VA, USA, 1980.
21. ANSYS® Academic Research, Release 14.5. Available online: <http://www.ansys.com/> (accessed on 21 February 2017).
22. Shih, T.-H.; Liou, W.W.; Shabbir, A.; Yang, Z.; Zhu, J. A New  $k-\epsilon$  Eddy-Viscosity Model for High Reynolds Number Turbulent Flows—Model Development and Validation. *Comput. Fluids* **1995**, *24*, 227–238. [[CrossRef](#)]
23. Reynolds, W.C. Fundamentals of Turbulence for Turbulence Modeling and Simulation. Available online: <http://www.dtic.mil/cgi-bin/GetTRDoc?Location=U2&doc=GetTRDoc.pdf&AD=ADP005793> (accessed on 28 February 2017).
24. Menter, F.R. Two-Equation Eddy-Viscosity Turbulence Models for Engineering Applications. *AIAA J.* **1994**, *32*, 1598–1605. [[CrossRef](#)]

